SUPPLEMENTARY METHODS

Materials

AZD1775 and AZD1775-D8 were provided by Astrazeneca (Delaware, MD). Cyclosporin A, loperamide, estrone 3-sulphate, sulfobromophthalein, and lucifer yellow were purchased from Sigma Aldrich Corporation (St. Louis, MO, USA). Midazolam and gefitinib were obtained from Toronto Research Chemicals Inc. (Ontario, Canada). Fluvastatin and Ko143 were purchased from Cayman Chemical (Ann Arbor, MI, USA). Pooled human liver and intestine microsomes and NADPH-regenerating system solutions A and B were purchased from Corning Inc. (Corning, NY, USA). Dulbecco's modified Eagle's medium (DMEM), DMEM GlutaMAX (Gibco 10566), Hank's balanced salt solution (HBSS), and fetal bovine serum (FBS) were purchased from Atlanta Biologicals (Flowery Branch, GA, USA). Pooled human plasma were purchased from Innovative Research Inc. (Novi, MI, USA)

Cell lines

Madin-Darby canine kidney II (MDCKII) cells with stable overexpression of ABCB1 (named MDCKII-ABCB1 cells) or ABCG2 (named MDCKII-ABCG2 cells) and the parental MDCKII cell line were provided by The Netherlands Cancer Institute (Amsterdam, Netherlands). These cell lines were maintained in DMEM GlutaMAX (Gibco 10566) supplemented with 10% FBS. Human embryonic kidney (HEK293) cells with stable overexpression of OATP2B1 or OAT3 as well as their respective vector control cell lines were provided by Dr. Alex Sparreboom (Ohio State University, Columbus, OH).

These cell lines were cultured in DMEM supplemented with 10% FBS. HEK293 cells with transient expression of OATP1A1 were generated by transiently transfecting HEK293 cells with a pCMV6-Entry vector expressing OATP1A2 from the CMV promoter (OriGene, Rockville, MD) or a GFP expression vector as the control. Cell transfection was performed using Lipofectamine 2000 according to the manufacturer's instruction (Invitrogen, Carlsbad, CA). The transport experiment was carried out 48 h after transfection. The expression of functional transporters in their respective cell lines were confirmed by western blot and functional experiments with known typical substrates.

In vitro experiments

In vitro Metabolism. *In vitro* metabolic kinetic parameters of AZD1775 were examined by incubating varying concentrations of AZD1775 (0.5 to 60 μM) with pooled human liver or intestine microsomes (0.4 mg/mL) at 37℃ for 30 min, as described previously with modifications (1,2). The kinetic profile of AZD1775 disappearance velocity versus initial drug concentrations was fitted to the Michaelis-Menton equation using the nonlinear regression analysis with Sigma Plot 12.0 (Systat Software, Inc., San Jose, CA). The *in vitro* intrinsic clearance (CL_{int}) was calculated as V_{max}/K_m, where V_{max} is maximum metabolic velocity and K_m is the substrate concentration at which 50% of V_{max} is obtained.

Transcellular permeability and interactions with efflux transporters. The MDCKII-MDR1 cell monolayer model has been widely used as an *in vitro* BBB model due to its simplicity and similar predictability as other *in vitro* models derived from human brain endothelia cells (3). AZD1775 passive transcellular permeability was determined using MDCKII cells, and its interaction with the efflux transporters ABCB1 and ABCG2 were assessed using MDCKII-MDR1 and MDCKII-BCRP cells,

respectively, as described previously with modifications (4,5). Briefly, cells (3×10^4 cells per well) were seeded into 96-well transwell inserts (0.4-μm pore size, polycarbonate membrane; Corning, Tewksbury, MA), and cultured in DMEM GlutaMAX (Gibco 10566) supplemented with 10% FBS for 4 – 5 days, with daily change of fresh medium. Bidirectional permeability experiments were performed on day 5. To determine the apical-to-basolateral (A→B) permeability, 100 μL HBSS containing AZD1775 (5 μM) was added into the top chamber and 220 μL drug-free HBSS was added into the bottom chamber. To determine the basolateral-to-apical (B→A) permeability, 100 μL drug-free HBSS was added into the top chamber and 220 μL HBSS containing AZD1775 (5 μM) was added into the bottom chamber. In addition, lucifer yellow (0.1 mg/mL) (a paracellular integrity marker) was added into each top chamber. After 1 h incubation at 37°C, samples were collected from both donor and receiver chambers. Lucifer yellow fluorescence in the receiver (bottom) chamber was measured using a fluorescence plate reader (PerkinElmer VICTOR^{TM}X3 2030 Multilabel Reader) with excitation and emission wavelengths of 485 and 535 nm, respectively. The permeability of lucifer yellow was calculated from fluorescence values as: permeability = (sample – HBSS blank) / (0.1 mg/mL lucifer yellow solution – HBSS blank), with a permeability of < 0.03 indicating the integrity of the cell monolayer. AZD1775 concentrations in both chambers were determined by a validated LC-MS/MS method (6).

Bidirectional permeability experiments for AZD1775 on parental MDCKII and MDCKII-ABCB1 or –ABCG2 cell monolayers were carried out in the absence and presence of cyclosporine A (10 μM; a typical inhibitor for ABCB1) or Ko143 (1 μM; a typical inhibitor for ABCG2) in the top chamber. In parallel, permeability experiments were performed for loperamide (5 μM) (a typical ABCB1 substrate) and gefitinib (1 μM) (a typical ABCG2 substrate) as the positive controls.

Apparent permeability (P_{app} [cm/s]) was calculated as: $P_{app} = [V_r/(S \times C_0)] \times dC_r/dt$, where V_r is the volume of medium (mL) in the receiver chamber, S is the surface area (cm^2) of the cell monolayer, C_0 is the initial drug concentration (μM) in the donor chamber, and dC_r/dt is the rate of drug permeation across the cell monolayer (μM/s). Efflux ratio (ER) was calculated as the ratio of basolateral-to-apical apparent permeability ($P_{app,B-A}$) to apical-to-basolateral apparent permeability ($P_{app,A-B}$). Net efflux ratio was the efflux ratio determined from MDCKII-MDR1 or MDCKII-BCRP cells divided by the efflux ratio determined from the parental MDCKII cells. The mass recovery was defined as the percentage of the total drug amount recovered from both donor and receiver chambers relative to the initial drug amount in the donor chamber.

pH-dependent permeability. It has been reported that the extracellular/interstitial milieu of brain tumors is relatively acidic (pH, 6.0 – 7.0) compared to blood circulation (pH, 7.4). To examine potential impact of acidic tumor interstitium on the BBB passive permeability and active efflux of AZD1775, bi-directional permeability experiments on MDCKII, MDCKII-ABCB1, and MDCKII-ABCG2 cell monolayers were performed in HBSS with pH adjusted to 7.4, 7.0, 6.5, or 6.0 in the basolateral chamber (mimicking brain tumor interstitium) and a fixed pH (7.4) in the apical chamber (mimicking blood circulation).

Cellular uptake. Potential interactions of AZD1775 with the uptake transporters OATP1A2, OATP2B1, and OAT3 were assessed in HEK293 cells with over-expression of OATP1A2, OATP2B1, or OAT3. For uptake experiments, OATP1A2-, OATP2B1-, or OAT3-overexpressing cells and their respective vector control cells were seeded in 6-well plates (1×10^6 cell/well). After 24 h culture, cells were washed once with HBSS and incubated in 1 mL HBSS containing 1 μM of AZD1775 in the

absence or presence of an inhibitor (i.e., 100 μM sulfobromophthalein for OATP1A2, 10 μM fluvastatin A for OATP2B1, or 50 μM probenecid for OAT3) at 37^{o}C for 3 min which was optimized by the preliminary experiment. In the meantime, positive control experiments were performed by incubating cells with 5 μM estrone 3-sulphate (a typical substrate for OATP1A2, OATP2B1, and OAT3) in the absence or presence of an inhibitor (i.e., 100 μM sulfobromophthalein for OATP1A2, 10 μM fluvastatin A for OATP2B1, or 50 μM probenecid for OAT3) at 37^{o}C for 10 min. At the end of incubation, cells were washed twice with ice-cold PBS, and cell pellets were collected and stored at -80^{o}C until LC-MS/MS analysis. Intracellular concentrations of AZD1775 and estrone 3-sulphate were determined by LC-MS/MS (6,7), and normalized to cellular protein concentrations.

Binding to plasma and brain tissues. The unbound fraction of AZD1775 in human plasma and brain tissue were determined for glioblastoma patient plasma and brain tumor samples (from the phase 0 trial), using a validated equilibrium dialysis method (6).

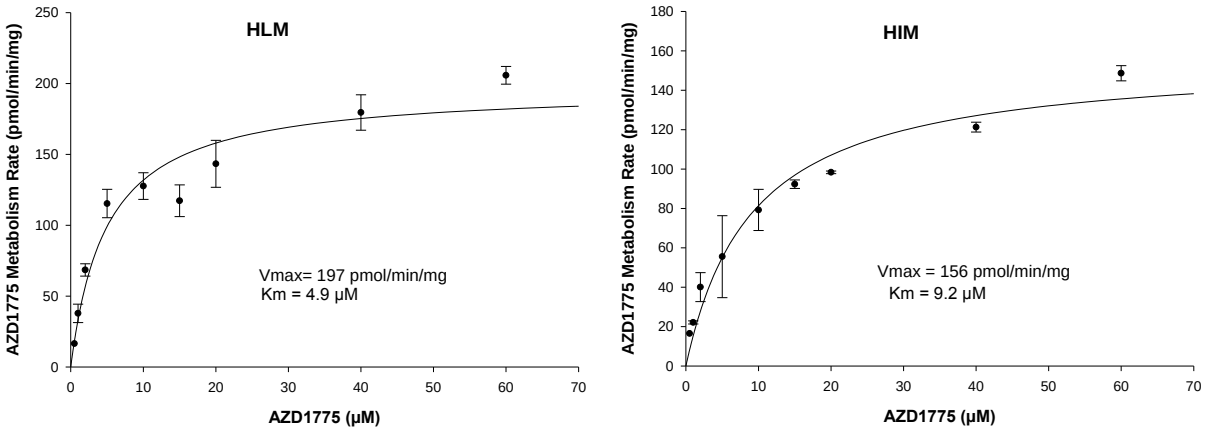

Supplementary Figure 1 Overall metabolic kinetics of AZD1775 in human liver and intestinal microsomes (HLM and HIM). The kinetic profile of AZD1775 disappearance velocity versus initial drug concentrations was fitted to the Michaelis-Menton equation using nonlinear regression analysis. Symbols represent the mean ± standard deviation of measured data from 3 independent experiments with duplicate in each experiment. V_{max} is maximum metabolic velocity and K_m is the substrate concentration at which 50% of V_{max} is obtained.

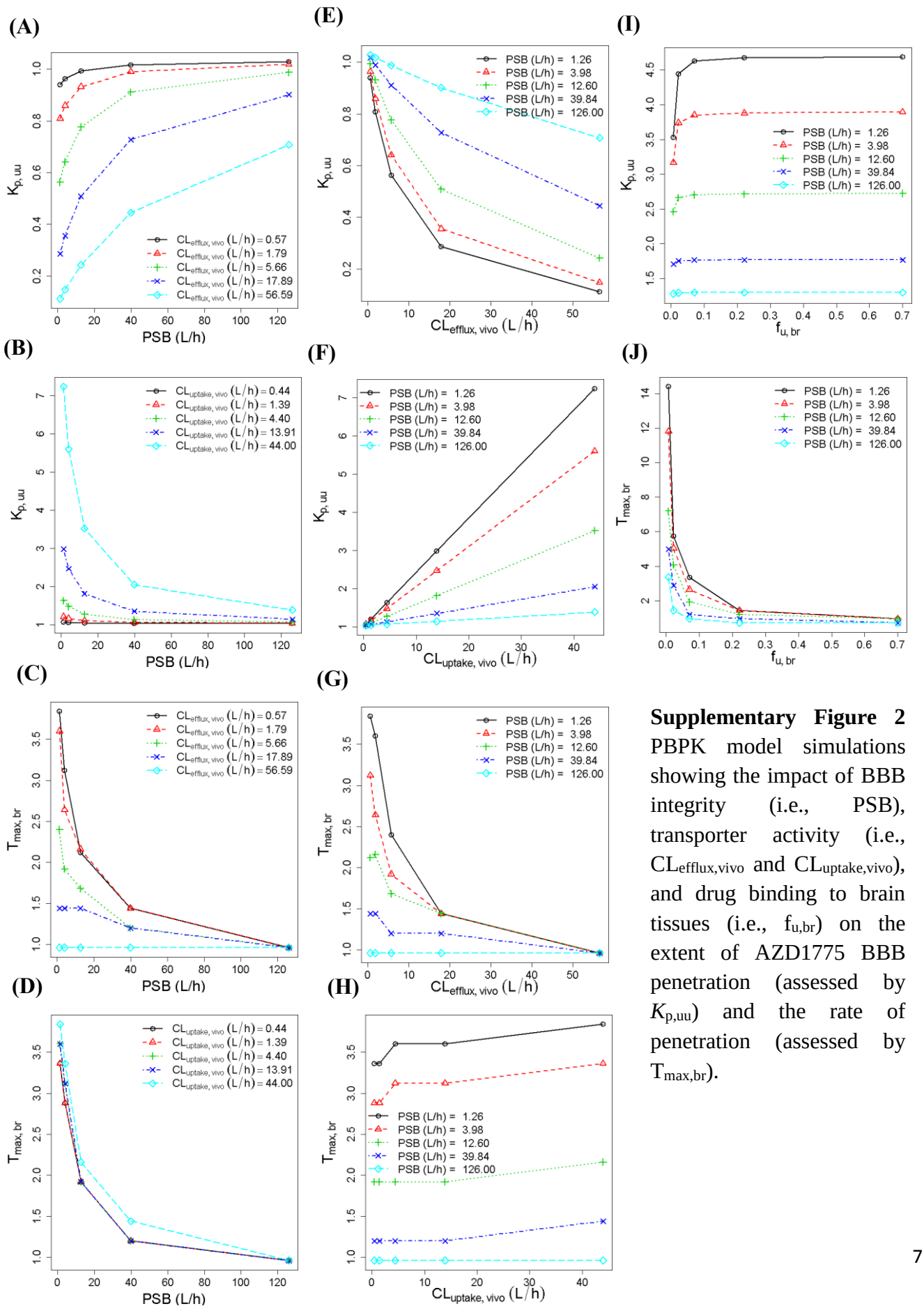

Supplementary Figure 2 PBPK model simulations showing the impact of BBB integrity (i.e., PSB), transporter activity (i.e., $CL_{efflux,vivo}$ and $CL_{uptake,vivo}$), and drug binding to brain tissues (i.e., $f_{u,br}$) on the extent of AZD1775 BBB penetration (assessed by $K_{p,uu}$) and the rate of penetration (assessed by $T_{max,br}$).

REFERENCES

1. Li J, Zhao M, He P, Hidalgo M, Baker SD. Differential metabolism of gefitinib and erlotinib by human cytochrome P450 enzymes. Clinical cancer research : an official journal of the American Association for Cancer Research **2007**;13(12):3731-7 doi 10.1158/1078-0432.CCR-07-0088.
2. Wu J, Shaw J, Dubaisi S, Valeriote F, Li J. In vitro metabolism and drug-drug interaction potential of UTL-5g, a novel chemo- and radioprotective agent. Drug metabolism and disposition: the biological fate of chemicals **2014**;42(12):2058-67 doi 10.1124/dmd.114.060095.
3. Hellinger E, Veszelka S, Toth AE, Walter F, Kittel A, Bakk ML, *et al.* Comparison of brain capillary endothelial cell-based and epithelial (MDCK-MDR1, Caco-2, and VB-Caco-2) cell-based surrogate blood-brain barrier penetration models. European journal of pharmaceutics and biopharmaceutics : official journal of Arbeitsgemeinschaft fur Pharmazeutische Verfahrenstechnik eV **2012**;82(2):340-51 doi 10.1016/j.ejpb.2012.07.020.
4. Di L, Whitney-Pickett C, Umland JP, Zhang H, Zhang X, Gebhard DF, *et al.* Development of a new permeability assay using low-efflux MDCKII cells. Journal of pharmaceutical sciences **2011**;100(11):4974-85 doi 10.1002/jps.22674.
5. Tolle-Sander S, Rautio J, Wring S, Polli JW, Polli JE. Midazolam exhibits characteristics of a highly permeable P-glycoprotein substrate. Pharmaceutical research **2003**;20(5):757-64.
6. Wu J, Sanai N, Bao X, LoRusso P, Li J. An aqueous normal-phase chromatography coupled with tandem mass spectrometry method for determining unbound brain-to-plasma concentration ratio of AZD1775, a Wee1 kinase inhibitor, in patients with glioblastoma. Journal of chromatography

B, Analytical technologies in the biomedical and life sciences **2016**;1028:25-32 doi 10.1016/j.jchromb.2016.05.050.

7. Hosogi J, Tanaka H, Fujita K, Kuwabara T, Ikegawa S, Kobayashi N, *et al.* LC-MS/MS coupled with immunoaffinity extraction for determination of estrone, 17beta-estradiol and estrone 3-sulfate in human plasma. Journal of chromatography B, Analytical technologies in the biomedical and life sciences **2010**;878(2):222-7 doi 10.1016/j.jchromb.2009.08.010.

List of Abbreviations:

ADAM model, Advanced Dissolution, Absorption and Metabolism model
AUC, area under concentration-time curve
B/P, blood-to-plasma partition ratio
BBB, blood-brain barrier
BMvPGB, milligrams of brain microvessels per gram brain
BW, brain weight
$CL_{ABCB1,vitro}$ and $CL_{ABCB1,vitro}$, ABCB1- and ABCG2-mediated in vitro efflux clearance, respectively
$CL_{efflux,BBB}$, efflux transporter-mediated efflux clearance at the BBB
$CL_{efflux,CSF}$, efflux transporter-mediated efflux clearance at the blood-cranial CSF barrier
$CL_{efflux,vitro}$, *in vitro* efflux transporter-mediated clearance
$CL_{efflux,vivo}$, *in vivo* efflux transporter-mediated clearance
CL_{int}, *in vitro* metabolic intrinsic clearance
CL_R, renal clearance
$CL_{uptake,BBB}$, uptake transporter-mediated uptake clearance at the BBB
$CL_{uptake,CSF}$, uptake transporter-mediated uptake clearance at the blood-cranial CSF barrier
$CL_{uptake,vivo}$, *in vivo* uptake transporter-mediated clearance
$C_{max,br}$, maximum drug brain concentration
CSF, cerebrospinal fluid
ER, efflux ratio
$f_{u,br}$, fraction unbound in brain tissue
$f_{u,p}$, fraction unbound in plasma
fu_{csf}, fraction unbound drug in CSF
fu_{gut}, fraction of unbound drug in enterocytes
fu_{mic}, fraction of unbound drug in in vitro microsomal incubation
IVIVE, in vitro-in vivo extrapolation
K_m, substrate concentration at which half of maximum metabolic rate is achieved
K_p, total drug brain-to-plasma partition coefficient
$K_{p,uu}$, unbound drug brain-to-plasma partition coefficient
logP, logarithm of the neutral species octanol-to-buffer partition ratio
MW, molecule weight
$P_{app,A-B}$, apical-to-basolateral apparent transcellular passive permeability
$P_{app,B-A}$, basolateral-to-apical apparent transcellular passive permeability
PBPK model, physiologically based pharmacokinetic model
$P_{eff,man}$, human intestinal effective permeability
PK_a, acid dissociation constant
PSB, passive permeability-surface area product at the BBB
PSC, passive permeability-surface area product at the blood-cranial CSF barrier
PSE, passive permeability-surface area product at the brain-cranial CSF barrier
PSE, passive permeability-surface area product at the brain-CSF barrier
Q_{BBB}, water transfer rate from the brain blood to brain mass
Q_{BCSFB}, CSF secretion rate by choroid plexus
$Q_{Brain,}$ cerebral blood flow rate linking the 4Bain model to the human whole body PBPK model
Q_{bulk}, bulk flow rate from brain mass to cranial CSF
Q_{gut}, gut blood flow

Q_{Sin} and Q_{Sout}, CSF shuttle flow rate between cranial and spinal compartment
Q_{sink}, CSF flow rate out of cranial and spinal compartments
RAF, relative activity factor
SA, human brain microvasculature surface area
$T_{max,br}$, time to achieve the maximum drug brain concentration
V_{max}, maximum metabolic rate
V_{ss}, volume of distribution at steady-state